

Simulating the Lipkin-Meshkov-Glick model in a hybrid quantum system

Yuan Zhou, Sheng-Li Ma, Bo Li, Xiao-Xiao Li, Fu-Li Li, and Peng-Bo Li*

*Shaanxi Province Key Laboratory of Quantum Information and Quantum Optoelectronic Devices,
Department of Applied Physics, Xian Jiaotong University, Xian 710049, China*

(Dated: December 10, 2021)

We propose an efficient scheme for simulating the Lipkin-Meshkov-Glick (LMG) model with nitrogen-vacancy (NV) center ensembles in diamond magnetically coupled to superconducting coplanar waveguide cavities. With the assistance of external microwave driving fields, we show that the interaction of the NV spins can be easily controlled, and several types of the LMG model can be realized by tuning the different parameters. Under the thermal dynamical limit, the distinct non-equilibrium second order quantum phase transition of the spin ensemble can be achieved at the critical point. Furthermore, we show that the spin squeezed state can be generated by tailoring the LMG Hamiltonian to possess the two-axis counter-twisting form in this hybrid quantum system.

I. INTRODUCTION

Manipulating the couplings of collective particles has been a fascinating subject with the development of new technologies for ultracold atoms, trapped ions, and solid-state spins [1–11]. One of the most important applications is to simulate the Lipkin-Meshkov-Glick (LMG) model in these different systems [12–14]. This model, which was first proposed in nuclear physics [15], has become a hot issue in the field of quantum information and quantum simulation [16–18]. Because of utilizing this model, we can not only manipulate the special quantum states such as the coherent spin state or spin squeezed state [19–22], but also “tailor” the microscopic interaction between the particles to mimic quantum phase transitions of the macroscopic system [16–18, 23]. In spite of many outstanding investigations for simulating the LMG model, it remains a challenge to realize the general LMG model in laboratory [20–23]. Therefore, it is appealing to present an experimentally feasible scheme for realizing the LMG model.

Recently, much attention has been paid to manipulating nitrogen-vacancy (NV) center ensembles in hybrid quantum systems [24–39]. NV centers in diamond have exhibited the excellent features such as fast microwave manipulation, optical preparation, and detection, and long coherence time even at room temperature [40–48]. Besides, we can directly combine NV centers with other quantum systems without requiring sophisticated trapping techniques [40, 41]. Therefore, hybrid quantum systems composed of superconducting circuits and NV centers have been extensively investigated [41–56]. Utilizing these hybrid systems, one can prepare fantastic quantum states, design quantum logic gates, store or transfer quantum states [24–29, 31–35, 44–49, 51, 56]. Furthermore, we can perform some quantum simulating tasks with this spin-photon system [33, 57, 58]. In a recent paper, a protocol for simulating the Dicke model and Dicke Lattice Model is proposed with the isotropy and anisotropy

NV center ensembles in the periodic superconducting microwave cavities respectively [59]. This prominent work demonstrates that hybrid quantum systems provide a realistic platform for studying characteristic phenomena of nonequilibrium quantum systems in various configurations.

In this work, we propose an experimentally feasible scheme for simulating the LMG model in a hybrid quantum system with an NV center ensemble in diamond coupled to superconducting coplanar waveguide cavities. Under the condition of large detunings as well as the bad cavity limit, we can obtain the generalized LMG model in this hybrid system. We discuss several forms of the LMG model by adjusting the parameters such as detunings, Rabi frequencies, coupling coefficients and so on. In particular, we focus on the positive field case $h > 0$ of the $\chi = 0$ LMG model with ferromagnetic interactions $\lambda > 0$. Under the thermal dynamical limit, the distinct non-equilibrium second order quantum phase transition of the coupled spins can be achieved at the critical point, as the magnitude of the interaction strength varies. On the other hand, the LMG model with the form of $H \sim \hat{J}_x^2, \hat{J}_y^2, \hat{J}_z^2$ or $H \sim (\hat{J}_x^2 - \hat{J}_y^2)$, corresponding to the one-axis twisting or two-axis counter-twisting Hamiltonian, can also be utilized for generating the spin squeezed state [19–23, 31, 51, 58, 61]. Therefore, by tailoring the LMG model with the two-axis counter-twisting form, we can prepare the spin squeezed state with high degree of squeezing based on this kind of interaction. Our work provides a realistic platform for implementing LMG-type models and for studying characteristic phenomena of nonequilibrium quantum systems with hybrid quantum systems.

II. THE MODEL

As illustrated in Fig. 1(a), in this hybrid quantum system two superconducting coplanar waveguide cavities are strongly coupled together with the coefficient $\epsilon \sim 10$ MHz. Meanwhile one of them is magnetically coupled to an NV center ensemble [40, 41, 55–59]. The energy level structure of the single NV center is shown

* lipengbo@mail.xjtu.edu.cn

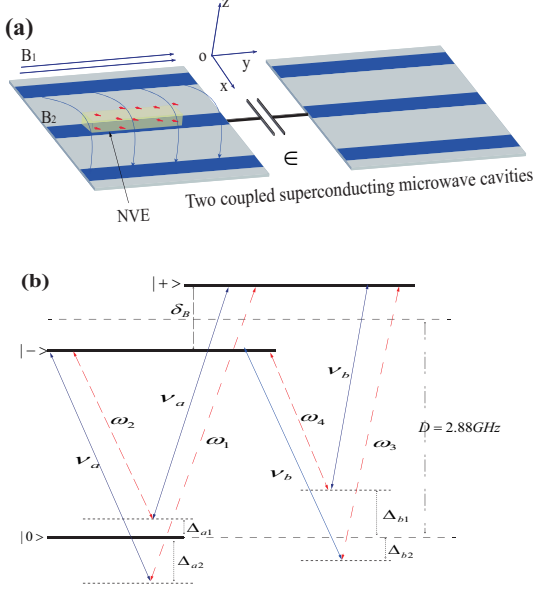


FIG. 1. (Color online) The scheme diagrams. (a) Two superconducting coplanar waveguide cavities are coupled together (the coupling coefficient is ϵ), an NV center ensemble is set in the center of one cavity and this ensemble is magnetically coupled to this cavity. (b) Level diagram of the NV center ground triplet state and the feasible four Raman transition channels. The blue solid arrows indicate the coupling to the two normal modes of the quantized cavities fields with the frequencies ν_a , and ν_b . The red dashed arrows show the four additional classical microwave fields with frequencies $\omega_1, \omega_2, \omega_3$, and ω_4 , and they are used to implement Raman transitions between the two excited spin states $|+\rangle$ and $|-\rangle$.

in Fig. 1(b). The electronic ground state is the spin triplet state denoted as $|m_s = 0, \pm 1\rangle$, and the zero-field splitting between the degenerate sublevels $|m_s = \pm 1\rangle$ and $|m_s = 0\rangle$ is $D = 2\pi \times 2.88 \text{ GHz}$. Then we apply a homogeneous static magnetic field B_1 to remove the degenerate states $|m_s = \pm 1\rangle$ with the Zeeman splitting $\delta_B/2\pi = 2g_e\mu_B B_1 \sim 100 \text{ MHz}$ ($g_e \simeq 2$ is the nitrogen-vacancy Landé factor, $\mu_B = 14 \text{ MHz mT}^{-1}$ is the Bohr magneton), which results in a three-level system denoted as $|m_s = 0\rangle \equiv |0\rangle$, $|m_s = +1\rangle \equiv |+\rangle$, and $|m_s = -1\rangle \equiv |-\rangle$.

In this solid-state system, the presence of local strain and the coupling of the NV spins to other electronic or nuclear spins in the surrounding can substantially generate the random frequency splitting δ_j between the states $|+\rangle$ and $|-\rangle$ for each NV center [59]. As a result, the coherence time is limited by this inhomogeneous broadening, resulting in an ensemble dephasing time T_2^* , which is about one microsecond according to the current experiments [62–64]. However, one can extend this coherence time from T_2^* to the value T_2 (close to the intrinsic spin coherence time) through the spin echo technology [62–64]. It has been reported that, the NV spin coherence time in an ensemble is comparable to that of single NV center, with $T_2 > 600 \mu\text{s}$ for a sample with natu-

ral abundance of ^{13}C and paramagnetic impurity density $\rho \sim 10^{15} \text{ cm}^{-3}$ [65, 66]. In this work, we have neglected these terms in the Hamiltonian and included their major influence via the dephasing rate γ_{dep} to the master equation equivalently.

Therefore, the Hamiltonian for describing these two cavities and the homogeneous NV center ensemble is ($\hbar = 1$)

$$H_1 = H_{NVE} + H_{10} + H_{NC} + H_{CC}, \quad (1)$$

where $H_{NVE} = \sum_{j=1}^N \omega_+ |+\rangle_j \langle +| + \omega_- |-\rangle_j \langle -|$ is the free Hamiltonian for the homogeneous NV ensemble, $H_{10} = \omega_{c1} \hat{c}_1^\dagger \hat{c}_1 + \omega_{c2} \hat{c}_2^\dagger \hat{c}_2$ is the free Hamiltonian for these two cavities with the destruction operators \hat{c}_i , ($i = 1, 2$), $H_{NC} = \sum_{j=1}^N [\eta_1 \hat{c}_1 |+\rangle_j \langle 0| + \eta_2 \hat{c}_1 |-\rangle_j \langle 0| + \text{h.c.}]$ is the interaction between cavity 1 and the NV centers, and $H_{CC} = \epsilon(\hat{c}_1 \hat{c}_2^\dagger + \hat{c}_1^\dagger \hat{c}_2)$ is the interaction between these two cavities. For the related parameters, N is the number of the available NV centers, $\omega_{\pm} = D \pm \delta_B/2$ the transition frequencies between the states $|\pm\rangle$ and $|0\rangle$, ω_{c1} and ω_{c2} the cavity mode frequencies, and η_1 and η_2 are the coupling strengths between the cavity mode \hat{c}_1 and the j th NV center for the transitions $|0\rangle_j \rightarrow |+\rangle_j$ and $|0\rangle_j \rightarrow |-\rangle_j$.

In order to acquire four distinct Raman transitions between the two spin states $|m_s = +1\rangle$ and $|m_s = -1\rangle$, we utilize the canonical transformation $\hat{c}_1 = (\hat{a} + \hat{b})/\sqrt{2}$, $\hat{c}_2 = (\hat{a} - \hat{b})/\sqrt{2}$, $\hat{c}_1^\dagger = (\hat{a}^\dagger + \hat{b}^\dagger)/\sqrt{2}$, and $\hat{c}_2^\dagger = (\hat{a}^\dagger - \hat{b}^\dagger)/\sqrt{2}$. As a result, we can get the equivalent form of the above Hamiltonian

$$H'_1 = \nu_a \hat{a}^\dagger \hat{a} + \nu_b \hat{b}^\dagger \hat{b} + H_{NVE} + \sum_{j=1}^N (g_1 \hat{a} |+\rangle_j \langle 0| + g_2 \hat{a} |-\rangle_j \langle 0| + g_3 \hat{b} |+\rangle_j \langle 0| + g_4 \hat{b} |-\rangle_j \langle 0| + \text{H.c.}), \quad (2)$$

where $\hat{a}(\hat{a}^\dagger)$ and $\hat{b}(\hat{b}^\dagger)$ are destruction (creation) operators for these two supermodes, g_k ($k = 1, 2, 3, 4$) are the relative average coupling coefficients between the supermodes and NV centers ($g_1 = g_3 = \eta_1/\sqrt{2}$, $g_2 = g_4 = \eta_2/\sqrt{2}$), and $\nu_a = \epsilon + (\omega_{c1} + \omega_{c2})/2$ and $\nu_b = -\epsilon + (\omega_{c1} + \omega_{c2})/2$ are the relative frequencies of these two supermodes respectively. Meanwhile, we introduce four microwave classical fields with frequencies ω_k ($k = 1, 2, 3, 4$) to the NV center ensemble, and neglect the NV centers' anisotropy and the deference from locations.

As a result, the total Hamiltonian for this hybrid quantum system can be expressed as

$$H_{\text{total}} = H_0 + H_{\text{int}}, \quad (3)$$

where

$$H_0 = \nu_a \hat{a}^\dagger \hat{a} + \nu_b \hat{b}^\dagger \hat{b} + \sum_{j=1}^N (\omega_+ |+\rangle_j \langle +| + \omega_- |-\rangle_j \langle -|),$$

$$\begin{aligned}
H_{\text{int}} = & \sum_{j=1}^N (g_1 \hat{a} |+\rangle_j \langle 0| + g_2 \hat{a} |-\rangle_j \langle 0| \\
& + g_3 \hat{b} |+\rangle_j \langle 0| + g_4 \hat{b} |-\rangle_j \langle 0| \\
& + \Omega_1/2 |+\rangle_j \langle 0| e^{-i\omega_1 t} + \Omega_2/2 |-\rangle_j \langle 0| e^{-i\omega_2 t} \\
& + \Omega_3/2 |+\rangle_j \langle 0| e^{-i\omega_3 t} + \Omega_4/2 |-\rangle_j \langle 0| e^{-i\omega_4 t} + \text{H.c.}).
\end{aligned}$$

In the interaction picture, we have

$$\begin{aligned}
H_I = & \sum_{j=1}^N (g_1 \hat{a} |+\rangle_j \langle 0| e^{i\Delta_{a1} t} + g_2 \hat{a} |-\rangle_j \langle 0| e^{-i\Delta_{a2} t} \\
& + g_3 \hat{b} |+\rangle_j \langle 0| e^{i\Delta_{b1} t} + g_4 \hat{b} |-\rangle_j \langle 0| e^{-i\Delta_{b2} t} \\
& + \Omega_1/2 |+\rangle_j \langle 0| e^{-i\Delta_{a2} t} + \Omega_2/2 |-\rangle_j \langle 0| e^{i\Delta_{a1} t} \\
& + \Omega_3/2 |+\rangle_j \langle 0| e^{-i\Delta_{b2} t} + \Omega_4/2 |-\rangle_j \langle 0| e^{i\Delta_{b1} t} + \text{H.c.}),
\end{aligned} \quad (4)$$

where $(\Delta_{a1} + \Delta_{a2}) \sim (\Delta_{b1} + \Delta_{b2}) \sim \delta_B$, $\Delta_{a1} = \omega_+ - \nu_a = \omega_- - \omega_2$, $\Delta_{a2} = \omega_1 - \omega_+ = \nu_a - \omega_-$, $\Delta_{b1} = \omega_+ - \nu_b = \omega_- - \omega_4$, and $\Delta_{b2} = \omega_3 - \omega_+ = \nu_b - \omega_-$. We assume that all of the fields are on the two-photon resonance in these four Raman transitions and take advantage of the relations $\delta_B \gg g_i, \Omega_i$, $|\Delta_{a1} \pm \Delta_{b1}| \gg g_i, \Omega_i$, and $|\Delta_{a2} \pm \Delta_{b2}| \gg g_i, \Omega_i$. In this case, the total effective Hamiltonian can be written as [60]

$$\begin{aligned}
H_{\text{eff}} = & \mu_0 \hat{J}_z + \zeta_a \hat{a}^\dagger \hat{a} + \zeta_b \hat{b}^\dagger \hat{b} + \eta_a^- \hat{J}_z \hat{a}^\dagger \hat{a} + \eta_b^- \hat{J}_z \hat{b}^\dagger \hat{b} \\
& + \frac{\sigma_a}{\sqrt{N}} (\hat{T}_a \hat{a} + \hat{T}_a^\dagger \hat{a}^\dagger) + \frac{\sigma_b}{\sqrt{N}} (\hat{T}_b \hat{b} + \hat{T}_b^\dagger \hat{b}^\dagger), \quad (5)
\end{aligned}$$

where the effective microscopic parameters are given by

$$\begin{aligned}
\mu_0 = & \frac{|g_1|^2}{\Delta_{a1}} - \frac{|g_2|^2}{\Delta_{a2}} + \frac{|g_3|^2}{\Delta_{b1}} - \frac{|g_4|^2}{\Delta_{b2}} \\
& + \frac{1}{4} \left(\frac{|\Omega_1|^2}{\Delta_{a2}} + \frac{|\Omega_2|^2}{\Delta_{a1}} - \frac{|\Omega_3|^2}{\Delta_{b2}} - \frac{|\Omega_4|^2}{\Delta_{b1}} \right), \\
\sigma_a \alpha_a = & \frac{\sqrt{N} g_1 \Omega_2^*}{2 \Delta_{a1}}, \sigma_a \beta_a = -\frac{\sqrt{N} g_2 \Omega_1^*}{2 \Delta_{a2}}, \\
\sigma_b \alpha_b = & \frac{\sqrt{N} g_3 \Omega_4^*}{2 \Delta_{b1}}, \sigma_b \beta_b = -\frac{\sqrt{N} g_4 \Omega_3^*}{2 \Delta_{b2}}, \\
\zeta_a = & \frac{N}{2} \left(\frac{|g_1|^2}{\Delta_{a1}} - \frac{|g_2|^2}{\Delta_{a2}} \right), \zeta_b = \frac{N}{2} \left(\frac{|g_3|^2}{\Delta_{b1}} - \frac{|g_4|^2}{\Delta_{b2}} \right), \\
\eta_a^- = & \left(\frac{|g_1|^2}{\Delta_{a1}} - \frac{|g_2|^2}{\Delta_{a2}} \right), \eta_b^- = \left(\frac{|g_3|^2}{\Delta_{b1}} - \frac{|g_4|^2}{\Delta_{b2}} \right). \quad (6)
\end{aligned}$$

The operators $\hat{T}_i = \alpha_i \hat{J}_+ + \beta_i \hat{J}_-$, $i = \{a, b\}$, and the dimensionless factors $\{\alpha_i, \beta_i\} \in [-1, 1]$ are introduced for convenience. The coefficients for the free Hamiltonian are μ_0 , ζ_a and ζ_b , and the coefficients for the interactions are $\sigma_i \alpha_i$ and $\sigma_i \beta_i$ ($i = \{a, b\}$), the coefficients for the nonlinear items are η_a and η_b , all of the coefficients above can be tuned by the number of NV centers N , the average coupling coefficients g_k , Rabi frequencies Ω_k^* ($k = 1, 2, 3, 4$) and the detunings. The collective ladder operators for the NV center ensemble are $\hat{J}_z = \frac{1}{2} \sum_{j=1}^N (|+\rangle_j \langle +| - |-\rangle_j \langle -|)$, $\hat{J}_+ = \sum_{j=1}^N |+\rangle_j \langle -|$, $\hat{J}_- = \sum_{j=1}^N |-\rangle_j \langle +|$, and they also satisfy the angular momentum commutation relations

$$[\hat{J}_i, \hat{J}_j] = i \varepsilon_{ijk} \hat{J}_k, [\hat{J}_+, \hat{J}_-] = 2 \hat{J}_z, [\hat{J}_z, \hat{J}_\pm] = \mp \hat{J}_\pm. \quad (7)$$

The master equation for the cavity modes and NV spins is,

$$\dot{\rho}_g = -i[H_{\text{eff}}, \rho_g] + \kappa_a D[\hat{a}] \rho_g + \kappa_b D[\hat{b}] \rho_g + \gamma_{\text{dep}} D[\hat{J}_z] \rho_g, \quad (8)$$

where $D[\hat{O}] \rho = 2\hat{O} \rho \hat{O}^\dagger - \hat{O}^\dagger \hat{O} \rho - \rho \hat{O}^\dagger \hat{O}$, κ_i is the cavity field decay rate, and γ_{dep} is the dephasing rate caused by the inhomogeneous broadening. Now we suppose that the two cavities are both bad cavities and satisfy the relations $\sqrt{\kappa_i^2 + \zeta_i^2} \gg \sigma_i, \mu_0$. Therefore, these two supermodes are only weakly excited and can be adiabatically eliminated from the dynamics [21, 23]. First of all, we set the subspace for the cavity supermodes as $|0_a 0_b\rangle = |1\rangle$, $|0_a 1_b\rangle = |2\rangle$, $|1_a 0_b\rangle = |3\rangle$, and $|1_a 1_b\rangle = |4\rangle$, and neglect populations of the highly excited states. As a result, the master equation (8) can be expressed as a set of coupled differential equations for the reduced density matrix elements, with $\rho = \text{Tr}_{\text{fields}}(\rho_g) = (\rho_{11} + \rho_{22} + \rho_{33} + \rho_{44})$. Owing to the strong damping, the most populated states of the supermodes are in the ground state $|1\rangle$ and the off-diagonal elements of the reduced density operator change slowly in time, i.e., $\dot{\rho}_{ij} = 0$, ($i \neq j$). Taking advantage of the steady solutions of the off-diagonal elements of ρ_{ij} , we have the following master equation for the reduced density operator

$$\dot{\rho} = -i[H, \rho] + \frac{\Gamma_a}{N} D[\hat{T}_a^\dagger] \rho + \frac{\Gamma_b}{N} D[\hat{T}_b^\dagger] \rho + \gamma_{\text{dep}} D[\hat{J}_z] \rho, \quad (9)$$

where

$$H = \mu_0 \hat{J}_z - \frac{\Lambda_a}{N} \hat{T}_a \hat{T}_a^\dagger - \frac{\Lambda_b}{N} \hat{T}_b \hat{T}_b^\dagger, \quad (10)$$

with $\Lambda_i = \frac{\sigma_i^2 \zeta_i}{\kappa_i^2 + \zeta_i^2}$, and $\Gamma_i = \frac{\sigma_i^2 \kappa_i}{\kappa_i^2 + \zeta_i^2}$. Because of the large cavity dissipations $\kappa_i \gg \eta_a^-, \eta_b^-$, the nonlinear terms of these two supermodes have no contributions in the adiabatic elimination course. According to the definition of \hat{T}_i and \hat{T}_i^\dagger , we transform the equation (10) into the generalized LMG model Hamiltonian [15–23, 61],

$$H_{\text{LMG}} = -2h \hat{J}_z - \frac{2\lambda}{N} (\hat{J}_x^2 + \chi \hat{J}_y^2), \quad (11)$$

where the parameters are given by

$$-2h = \mu_0 - \frac{\zeta_a((L_\alpha^a)^2 - (L_\beta^a)^2)}{N K_a} - \frac{\zeta_b((L_\alpha^b)^2 - (L_\beta^b)^2)}{N K_b},$$

$$2\lambda = \frac{\zeta_a(L_\alpha^a + L_\beta^a)^2}{K_a} + \frac{\zeta_b(L_\alpha^b + L_\beta^b)^2}{K_b},$$

$$\chi = \frac{K_b \zeta_a (L_\alpha^a - L_\beta^a)^2 + K_a \zeta_b (L_\alpha^b - L_\beta^b)^2}{K_b \zeta_a (L_\alpha^a + L_\beta^a)^2 + K_a \zeta_b (L_\alpha^b + L_\beta^b)^2},$$

$$K_a = (\kappa_a^2 + \zeta_a^2), K_b = (\kappa_b^2 + \zeta_b^2),$$

$$L_\alpha^a = \sigma_a \alpha_a, L_\beta^a = \sigma_a \beta_a, L_\alpha^b = \sigma_b \alpha_b, L_\beta^b = \sigma_b \beta_b.$$

These parameters can be controlled by adjusting the relevant parameters such as the detunings, Rabi frequencies, and coupling coefficients.

TABLE I. The relevant parameters for the specific LMG Hamiltonian

Parameters (MHz)	Two-axis counter-twisting LMG model (Equation (12))	Isotropic LMG model (Equation (14))	One-axis twisting LMG model (Equation (16))
$\sqrt{N}g_k(N \simeq 10^{12})$	12	12	12
$ \Omega_1^* /2\pi$	4	0	7
$ \Omega_2^* /2\pi$	1	1	3
$ \Omega_3^* /2\pi$	1	1	0.77
$ \Omega_4^* /2\pi$	4	0	0
$ \Delta_{a1} /2\pi$	20	20	30
$ \Delta_{a2} /2\pi$	80	80	70
$ \Delta_{b1} /2\pi$	80	80	50
$ \Delta_{b2} /2\pi$	20	20	50
$\sigma_a\alpha_a/2\pi$	0.3	0.3	0.6
$\sigma_a\beta_a/2\pi$	0.3	0	0.6
$\sigma_b\alpha_b/2\pi$	0.3	0	0
$\sigma_b\beta_b/2\pi$	-0.3	0.3	0.092

In addition, we consider several forms of the LMG model by tuning these parameters. In order to describe them more clearly, we list three groups of parameters in TABLE. I. Then we can get several different forms of the LMG Hamiltonian via choosing the suitable parameters. When we set the parameters as those in the first column of TABLE. I, we can get the conventional LMG Hamiltonian with the expression

$$H = -2h\hat{J}_z - \frac{2\lambda}{N}(\hat{J}_x^2 - \hat{J}_y^2), \quad (12)$$

where $h = -\mu_0/2$, $\chi = -1$, $\alpha_a = \alpha_b = \alpha = \sqrt{2}/2$, $\beta_a = -\beta_b = \beta = \sqrt{2}/2$, $\lambda = \Lambda_a = -\Lambda_b$, and $\sigma_a \simeq \sigma_b$. The master equation reduces to the form

$$\dot{\rho} = -i[H, \rho] + \frac{2\Gamma_a\alpha^2}{N}D[\hat{J}_-]\rho + \frac{2\Gamma_b\beta^2}{N}D[\hat{J}_+]\rho + \gamma_{\text{dep}}D[\hat{J}_z]\rho. \quad (13)$$

This kind of LMG model has been investigated for phase transitions and multiparticle entanglement [12–17]. One can generate the spin squeezed state by the two-axis counter-twisting interactions utilizing this kind of Hamiltonian [19–21].

Secondly, we can get the isotropic Hamiltonian when choosing the second column parameters in TABLE. I.

$$H = -2h\hat{J}_z - \frac{2\lambda}{N}(\hat{J}_x^2 + \hat{J}_y^2), \quad (14)$$

where $h = -\mu_0/2$, $\chi = 1$, $\Lambda_a = \Lambda_b \equiv \lambda$, $\alpha_a = \beta_b = 1$, $\alpha_b = \beta_a = 0$ and $\sigma_a \simeq \sigma_b$. Then the master equation is

$$\dot{\rho} = -i[H, \rho] + \frac{\Gamma_a}{N}D[\hat{J}_-]\rho + \frac{\Gamma_b}{N}D[\hat{J}_+]\rho + \gamma_{\text{dep}}D[\hat{J}_z]\rho. \quad (15)$$

This is an isotropic LMG Hamiltonian which can be solved exactly because of $H = -2h\hat{J}_z - 2\lambda\hat{\mathbf{J}}^2/N + 2\lambda\hat{J}_z^2/N$, where $\hat{\mathbf{J}}^2 = \hat{J}_x^2 + \hat{J}_y^2 + \hat{J}_z^2$. We can get the double degenerate ground states for this Hamiltonian when $h = 0$. Otherwise, for the symmetry breaking case $h \neq 0$,

we will get an unique ground state ($h > 0$, $|\uparrow\uparrow\uparrow \dots\rangle = |m_z = N/2\rangle$) or ($h < 0$, $|\downarrow\downarrow\downarrow \dots\rangle = |m_z = -N/2\rangle$). In addition there will be the transition between the ferromagnetic and antiferromagnetic interactions by tuning the sign of λ when we set $h = 0$, and so on.

Finally, we can obtain the simple Hamiltonian according to the third column in TABLE. I,

$$H = -2h\hat{J}_z - \frac{2\lambda}{N}\hat{J}_x^2, \quad (16)$$

and achieve the master equation

$$\dot{\rho} = -i[H, \rho] + \frac{\Gamma_a}{N}D[2\hat{J}_x]\rho + \frac{\Gamma_b}{N}D[\hat{J}_+]\rho + \gamma_{\text{dep}}D[\hat{J}_z]\rho, \quad (17)$$

where $\lambda = 2\Lambda_a$, $\chi = 0$, $\alpha_a = \beta_a = 1$, $\beta_b = \sqrt{2}/2$, and $\alpha_b = 0$. There will be many other applications of this kind of interactions, e.g., simulating the first order and second order phase transitions, preparing multiparticle entanglement and generating spin squeezed state by the one-axis twisting interactions [12–14]. In the following, we will investigate this kind of phase transition in this hybrid quantum system for the Hamiltonian with the form given by equation (16).

III. THE SECOND-ORDER PHASE TRANSITION

Under the thermodynamic limit corresponding to that $N \rightarrow \infty$, $V \rightarrow \infty$, and the density $n = N/V$ keeps finite, we can neglect the quantum fluctuation for this spin-spin interaction system, for example, $\langle \hat{J}_k \hat{J}_l \rangle \rightarrow \langle \hat{J}_k \rangle \langle \hat{J}_l \rangle$, where $k, l \in \{x, y, z\}$. Considering the ferromagnetic interactions ($\lambda > 0$) from equation (16), we will apply the method of semiclassical equations of motion to simulate the second-order quantum phase transition. The differential equations of motion for the expectation values of collective spin components $\langle \hat{J}_i \rangle = \text{Tr}(\rho \hat{J}_i)$ are readily derived from the master equation (17). Utilizing the relations $d\langle \hat{J}_i \rangle/dt = \text{Tr}(\dot{\rho} \hat{J}_i)$ and the definition of

$X = \langle \hat{J}_x \rangle / j$, $Y = \langle \hat{J}_y \rangle / j$, and $Z = \langle \hat{J}_z \rangle / j$ ($j = N/2$ is the scaling factor), we obtain the semiclassical equations of motion

$$\dot{X} = 2hY - \Gamma_b ZX - \gamma_{\text{dep}} X / 2 \quad (18)$$

$$\dot{Y} = -2hX + 2\lambda ZX - \Gamma_b ZY - \gamma_{\text{dep}} Y / 2 \quad (19)$$

$$\dot{Z} = -2\lambda XY + \Gamma_b (X^2 + Y^2). \quad (20)$$

These three formulas can not form a closed set of group, and the constraint $X^2 + Y^2 + Z^2 = 1$ corresponds to the conservation of angular momentum. Therefore, we can get a closed set of group with these four equations, and obtain the steady-state analytical solutions or numerical solutions from these equations. The numerical solutions for the finite N will lead to $\langle \hat{J}_x \rangle = \langle \hat{J}_y \rangle = 0$ for all λ . Then we will derive the steady-state analytical solutions of motion from these equations

$$2hY - \Gamma_b ZX - \gamma_{\text{dep}} X / 2 = 0, \quad (21)$$

$$-2hX + 2\lambda ZX - \Gamma_b ZY - \gamma_{\text{dep}} Y / 2 = 0, \quad (22)$$

$$-2\lambda XY + \Gamma_b (X^2 + Y^2) = 0, \quad (23)$$

$$X^2 + Y^2 + Z^2 = 1. \quad (24)$$

We solve the equations (21)-(24) and find the critical point of the coupling strength λ ,

$$\lambda_c = h + \frac{\Gamma_b^2}{4h}. \quad (25)$$

It is obviously that the critical point λ_c is varying with Γ_b and h , but immune to the dephasing γ_{dep} .

When the coupling strength satisfies $\lambda < \lambda_c$, the steady-state belongs to the normal phase and the analytical solutions of motion are given by

$$Z_{np} = 1, X_{np} = Y_{np} = 0. \quad (26)$$

While for $\lambda > \lambda_c$, which is the region for the second-order phase transition, the steady-state corresponds to the broken phase and the analytical solutions are given by

$$Z_{bp} = Z_0 - r_0, \quad (27)$$

$$X_{bp} = \pm \sqrt{\frac{1 - (Z_0 - r_0)^2}{1 + \Gamma_b Z_0^2 / 2h}}, \quad (28)$$

$$Y_{bp} = \pm \frac{\Gamma_b}{2h} Z_0 \left(\sqrt{\frac{1 - (Z_0 - r_0)^2}{1 + \Gamma_b Z_0^2 / 2h}} \right), \quad (29)$$

where $Z_0 = \frac{2h}{\Gamma_b^2} (\lambda - \sqrt{\lambda^2 - \Gamma_b^2 (1 + r_0 \lambda / h)})$, and the dimensionless parameter $r_0 = \gamma_{\text{dep}} / 2\Gamma_b$. The analytical solutions of motion exhibit a bifurcation at the critical coupling strength λ_c .

In order to exhibit the macroscopic difference between the normal phase and the broken phase, we can apply the Bloch vector to describe the average collective spins. The NV center ensemble in this system can be interpreted as

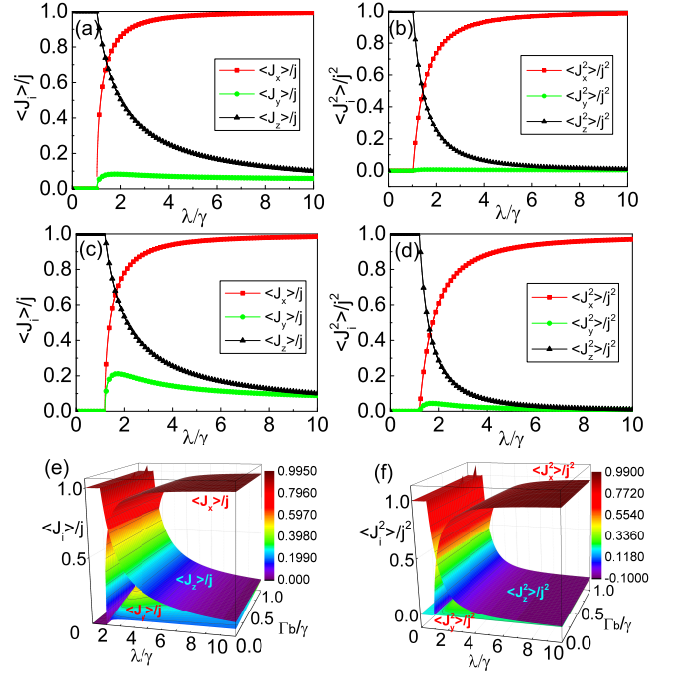


FIG. 2. (Color online) The average values of the first-order spin components and the quadratic spin components versus the dimensionless variables λ/γ and Γ_b/γ , where the parameters are chosen as $\gamma_{\text{dep}} = 0.2\gamma$ and $h = \gamma$. The average values of $\langle \hat{J}_i \rangle / j$ and $\langle \hat{J}_i^2 \rangle / j^2$ versus λ/γ with $\Gamma_b = 0.2\gamma$ for (a) – (b) and $\Gamma_b = 0.8\gamma$ for (c) – (d). (e) – (f) The three dimensional plots of $\langle \hat{J}_i \rangle / j$ and $\langle \hat{J}_i^2 \rangle / j^2$ versus $(\lambda/\gamma, \Gamma_b/\gamma)$.

the collective spin-1/2 particle system. According to the definition of spin vacuum state and spin coherent state [19], the average value of the spin ensemble can be expressed as $X = \sin \theta \cos \phi$, $Y = \sin \theta \sin \phi$, and $Z = \cos \theta$, where the vector $(1, \theta, \phi)$ means the average-spin direction for this spin ensemble. According to this definition, we can describe the macroscopic eigenstate as $|\theta, \phi\rangle$. When we set $\theta = 0$, the average value is $Z = 1$, $X = 0$, and $Y = 0$, which means the average-spin direction is along $+z$ axis and the spin ensemble belongs to the normal phase area. On the other hand, if $\theta \neq 0$, the average value is $Z = \cos \theta$, $X = \sin \theta \cos \phi$, and $Y = \sin \theta \sin \phi$, which means the Bloch vector is rotated away from $+z$ axis and then the system falls in the broken phase area. The second-order phase transition will occur in this area when $\lambda = \lambda_c$.

In this setup, we assume that the density of the NV centers is about $\varrho \sim 10^{15} \text{cm}^{-3}$ with the total number $N \sim 10^{12}$, and we set the parameters as the last column for the simple LMG model in TABLE. I. We can calculate the expectation values of the spin components of the Bloch vector numerically from the equations (21)–(24), where the effective coupling strengths $\lambda \sim 2\pi \times 0.25$ MHz and $h \sim 2\pi \times 0.25$ MHz, the effective dissipation rate $\Gamma_b \sim 2\pi \times 0.05$ MHz and the dephasing rate $\gamma_{\text{dep}} \sim 2\pi \times 0.02$ MHz. The scaling factor is $\gamma \sim 2\pi \times 0.25$

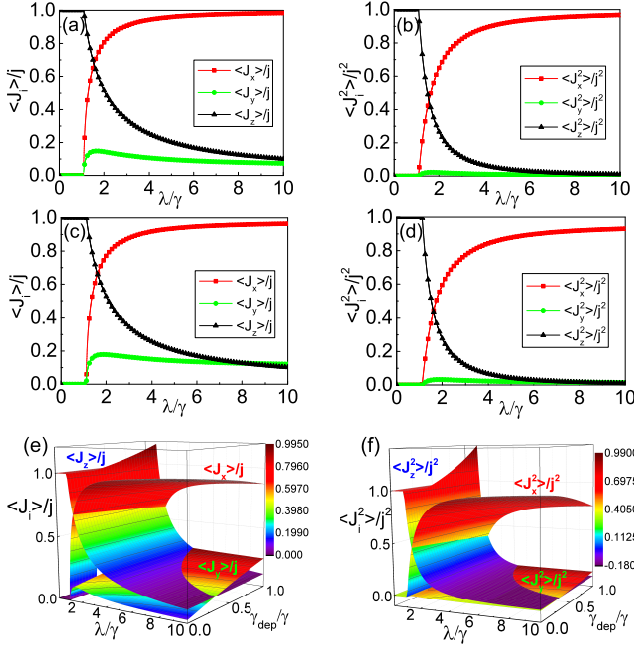


FIG. 3. (Color online) The average values of the first-order spin components and the quadratic spin components versus the dimensionless variables λ/γ and $\gamma_{\text{dep}}/\gamma$, where the parameters are chosen as $\Gamma_b = 0.5\gamma$ and $h = \gamma$. The average values of $\langle \hat{J}_i \rangle / j$ and $\langle \hat{J}_i^2 \rangle / j^2$ versus λ/γ with $\gamma_{\text{dep}} = 0.2\gamma$ for (a) – (b) and $\gamma_{\text{dep}} = 0.4\gamma$ for (c) – (d). (e) – (f) The three dimensional plots of $\langle \hat{J}_i \rangle / j$ and $\langle \hat{J}_i^2 \rangle / j^2$ versus $(\lambda/\gamma, \gamma_{\text{dep}}/\gamma)$.

MHz.

In order to illustrate the effects of the coupling λ , the dissipation Γ_b and the dephasing γ_{dep} on phase transitions, in Figs. 2 and 3 we present the average values of the first-order spin components and the quadratic spin components under different conditions from equations (26)–(29).

As shown in Fig. 2(a), (b), (c) and (d), we set $\gamma_{\text{dep}} = 0.2\gamma$ and $h = \gamma$, and get the curve for the average values of the first-order $\langle \hat{J}_i \rangle / j$ and the quadratic $\langle \hat{J}_i^2 \rangle / j^2$ spin components varying with λ/γ , where $\Gamma_b = 0.2\gamma$ (Fig. 2 (a) and (b)) and $\Gamma_b = 0.8\gamma$ (Fig. 2(c) and (d)). In Fig. 2(e) and (f), we also display the three dimensional surface of these average values varying with the two parameters $(\lambda/\gamma, \Gamma_b/\gamma)$ when $\gamma_{\text{dep}} = 0.2\gamma$ and $h = \gamma$. One can find that the second-order phase transition occurs at the point near λ_c . It is shown that the average value of $\langle \hat{J}_z \rangle / j$ or $\langle \hat{J}_z^2 \rangle / j^2$ is always 1 when $\lambda < \lambda_c$, and then displays a discontinuous transition as λ/γ increases to a value larger than 1. As for the $\langle \hat{J}_x \rangle / j$ or $\langle \hat{J}_x^2 \rangle / j^2$ component, it exhibits a reversed behavior compared to the $\langle \hat{J}_z \rangle / j$ or $\langle \hat{J}_z^2 \rangle / j^2$ component. However, both display the discontinuous behaviour at the point λ_c , which signifies quantum phase transition occurs. In addition, as shown in Fig. 2(e) and (f), when the dissipation Γ_b increases, the critical point λ_c will be slightly shifted. The value

of $\langle \hat{J}_y \rangle / j$ or $\langle \hat{J}_y^2 \rangle / j^2$ in the vicinity of λ_c also increases a little. Comparing Fig. 2(a) or (b) with Fig. 2(c) or (d), the critical point has changed from about $\lambda_c = 1.01\gamma$ to $\lambda_c = 1.16\gamma$. Moreover, in the vicinity of λ_c , the value of $\langle \hat{J}_y \rangle / j$ has changed from a value less than 0.1 to one larger than 0.2.

In Fig. 3(a), (b), (c) and (d), we set $\Gamma_b = 0.5\gamma$ and $h = \gamma$, and can obtain the illustrations for the values of the first-order $\langle \hat{J}_i \rangle / j$ and the quadratic $\langle \hat{J}_i^2 \rangle / j^2$ spin components varying with λ/γ , where $\gamma_{\text{dep}} = 0.2\gamma$ (Fig. 3a) and (b)) or $\gamma_{\text{dep}} = 0.4\gamma$ (Fig. 3(c) and (d)). Moreover, as shown in Fig. 3(e) and (f), we also plot the three dimensional surface of these average values varying with the parameters $(\lambda/\gamma, \gamma_{\text{dep}}/\gamma)$ when $\Gamma_b = 0.5\gamma$ and $h = \gamma$. We can obtain the critical point for the phase transition $\lambda_c = 1.0625\gamma$ from Fig. 3, which is immune to the dephasing γ_{dep} . Figure. 3 displays the same behavior of the average spin components as in Fig. 2. We find a discontinuous behavior as λ increases to a value larger than λ_c , and $\langle \hat{J}_x \rangle / j$ or $\langle \hat{J}_x^2 \rangle / j^2$ exhibits a reversed behavior compared to $\langle \hat{J}_z \rangle / j$ or $\langle \hat{J}_z^2 \rangle / j^2$. Although the dephasing will not affect the critical point, we can not neglect its effect on the phase transition. As shown in Fig. 3(e) and (f), when increasing λ and γ_{dep} , the values of $\langle \hat{J}_y \rangle / j$ will be enlarged continuously. Meanwhile $\langle \hat{J}_x \rangle / j$ will be suppressed continuously too. When $\lambda/\gamma \sim 10$ and $\gamma_{\text{dep}}/\gamma \sim 1$, $\langle \hat{J}_y \rangle / j$ will keep the value of 0.24, while $\langle \hat{J}_x \rangle / j$ will be about 0.87. Therefore, we can simulate the second-order quantum phase transition with this hybrid quantum system, which provides the very convincing evidence for manipulating the spin ensembles realistically in our scheme.

IV. THE SPIN SQUEEZED STATE

It is known that spin squeezed states can be prepared efficiently by one-axis twisting or two-axis counter-twisting interactions [19]. These kinds of interactions are equivalent to the LMG model with the form of equation (16) or (12). Although the two-axis counter-twisting Hamiltonian is superior to the one-axis twisting one, the spin-spin interaction with the form of two-axis counter-twisting has not been realized in any experiments due to the demanding requirements [19–22, 61]. We will discuss how to prepare spin squeezed states by simulating the two-axis counter-twisting interaction with equation (12) in our scheme. In this system, the coherent coupling strength between a single NV center and the cavity is much less than the cavity dissipation rates ($|g_i| \ll \kappa_{a,b}$), but this collective coupling can be enhanced by increasing the number of the NV centers. Therefore, we can neglect the dissipations as long as the condition $\sqrt{N}|g_i| \gg \kappa_{a,b}$ is satisfied.

In order to describe the degree of spin squeezing, we introduce the definition [61]

$$\xi^2 = \frac{4 \min(\Delta \hat{J}_{n\perp}^2)}{N}, \quad (30)$$

where \vec{n}_\perp refers to an axis perpendicular to the mean-spin direction, and the term “min” is the minimization over all directions \vec{n}_\perp . The first step is to determine the mean-spin direction \vec{n}_0 by the expectation values $\langle \hat{J}_\alpha \rangle$, with $\alpha \in \{x, y, z\}$. We write \vec{n}_0 with spherical coordinates $\vec{n}_0 = (\sin \theta \cos \phi, \sin \theta \sin \phi, \cos \theta)$, and this description is equivalent to the coherent spin state $|\theta, \phi\rangle$. We can get the other two orthogonal bases which are perpendicular to \vec{n}_0 ,

$$\vec{n}_1 = (-\sin \phi, \cos \phi, 0), \quad (31)$$

$$\vec{n}_2 = (\cos \theta \cos \phi, \cos \theta \sin \phi, -\sin \theta). \quad (32)$$

Hence, $\vec{n}_\perp = \vec{n}_1 \cos \beta + \vec{n}_2 \sin \beta$ is the arbitrary direction vector perpendicular to \vec{n}_0 , and we can find a pair of optimal quadrature operators by tuning β . Then we obtain two components of the angular momentum,

$$\hat{J}_{\vec{n}_1} = -\sin \phi \hat{J}_x + \cos \phi \hat{J}_y, \quad (33)$$

$$\hat{J}_{\vec{n}_2} = \cos \theta \cos \phi \hat{J}_x + \cos \theta \sin \phi \hat{J}_y - \sin \theta \hat{J}_z. \quad (34)$$

As a result, we acquire the expression of the optimal squeezing parameter

$$\xi^2 = \frac{2}{N} [\langle \hat{J}_{\vec{n}_1}^2 + \hat{J}_{\vec{n}_2}^2 \rangle - \sqrt{(\langle \hat{J}_{\vec{n}_1}^2 - \hat{J}_{\vec{n}_2}^2 \rangle)^2 + 4\text{Cov}(\hat{J}_{\vec{n}_1}, \hat{J}_{\vec{n}_2})}], \quad (35)$$

where

$$\text{Cov}(\hat{J}_{\vec{n}_1}, \hat{J}_{\vec{n}_2}) = \frac{1}{2} \langle \hat{J}_{\vec{n}_1} \hat{J}_{\vec{n}_2} + \hat{J}_{\vec{n}_2} \hat{J}_{\vec{n}_1} \rangle.$$

We can distinguish between spin coherent states and spin squeezed states distinctly for this NV center ensemble according to $\xi^2 = 1$ or $\xi^2 < 1$. Therefore, it is imperative for us to carry out some numerical calculations for the squeezing parameter in this system.

It is evident that one can strengthen the spin squeezing degree by increasing the total number of the spins [20–22, 45, 61]. As discussed above, we can get the relations $\sigma_a \alpha_a \simeq \sigma_a \beta_a$, $\sigma_b \alpha_b \simeq -\sigma_b \beta_b$ by tuning the collective couplings, the Rabi frequencies, and the detunings. Then we can get $\alpha = \beta = \sqrt{2}/2$ when setting $\sigma_a \simeq \sqrt{2}\sigma_a \alpha_a$, $\sigma_b \simeq \sqrt{2}\sigma_b \alpha_b$. We investigate equations (12) and (13) and assume that the coefficients are $\lambda \equiv |\Lambda_a| = |\Lambda_b|$, $\sigma_a \simeq \sigma_b \equiv \sigma$, $\zeta_a \simeq \zeta_b \equiv \zeta$, and the dissipations of the supermodes are $\kappa_a = \kappa_b \equiv \kappa$.

We choose the first column parameters for the conventional LMG model in TABLE. I and assume the dissipations $\kappa \sim 2\pi \times 0.1$ MHz. We choose the number of NV centers $N \simeq 10^6$ and get the collective coupling $\sqrt{N}g_i \simeq 2\pi \times 12$ kHz. Then the effective coupling coefficient is $\lambda = \sigma^2|\zeta|/(\kappa^2 + \zeta^2) \simeq \sigma^2|\zeta|/\kappa^2 \simeq 0$ Hz and the effective dissipations are $\Gamma_{a,b} = \sigma^2\kappa/(\kappa^2 + \zeta^2) \simeq \sigma^2/\kappa \simeq 2\pi \times 1.8$ Hz. So we can not prepare the spin squeezed state when $N \simeq 10^6$, because λ and $\Gamma_{a,b}$ are too weak. When we set $N \simeq 10^{10}$ and the collective coupling as $\sqrt{N}g_i \simeq 2\pi \times 1.2$ MHz, utilizing the same parameters above, we can get the effective coupling coefficient as $\lambda = \sigma^2|\zeta|/(\kappa^2 + \zeta^2) \simeq 2\pi \times 4.43$ kHz and the effective

dissipations as $\Gamma_{a,b} = \sigma^2\kappa/(\kappa^2 + \zeta^2) \simeq 2\pi \times 16.4$ kHz. It is evident that we can not prepare the spin squeezed state unless $N > 10^{10}$. On the other hand, if we choose $N \simeq 10^{12}$ and utilize the same parameters above, we find that, the effective coupling $\lambda \sim 2\pi \times 65.2$ kHz is much stronger than the effective dissipations $\Gamma_{a,b} \sim 2\pi \times 2.4$ kHz. Therefore, one can not prepare the spin squeezed state unless $N > 10^{10}$ in this setup. These estimations above also show that the appropriate choice for simulating spin squeezed state is $N \simeq 10^{12}$.

In the condition of weak excitations and $N \gg 1$, we map the collective spin operators $\hat{J}_+(\hat{J}_-)$ into the boson operators $\hat{d}^\dagger(\hat{d})$ in the Holstein-Primakoff representation,

$$\begin{aligned} \hat{J}_+ &= \sqrt{N}\hat{d}^\dagger, \\ \hat{J}_- &= \sqrt{N}\hat{d}, \\ \hat{J}_z &= (\hat{d}^\dagger\hat{d} - \frac{N}{2}), \end{aligned} \quad (36)$$

where the operators \hat{d} and \hat{d}^\dagger obey the standard boson commutator $[\hat{d}, \hat{d}^\dagger] = 1$. The equations (12) and (13) can be transformed as

$$\dot{\rho} = -i[H_T, \rho] + \Gamma_a D[\hat{d}]\rho + \Gamma_b D[\hat{d}^\dagger]\rho + \gamma_{\text{dep}} D[\hat{d}^\dagger\hat{d}]\rho, \quad (37)$$

$$H_T = -2h\hat{d}^\dagger\hat{d} - \lambda\hat{d}^2 - \lambda\hat{d}^{\dagger 2}. \quad (38)$$

We assume the collective spins are initially prepared in the state $|\theta = 0\rangle$ ($Z = 1$) and the dissipations satisfy $\Gamma_a = \Gamma_b$. Then we solve the master equation (37) numerically and present the simulations in Fig. 4. In this numerical simulation, the parameters are set as those in the first column of TABLE. I. With these parameters, we can obtain the effective coupling coefficient $\lambda \simeq 2\pi \times 65$ kHz, and the corresponding effective dissipations $\Gamma_{a,b} \simeq 2\pi \times 0.065$ kHz, $2\pi \times 0.65$ kHz and $2\pi \times 6.5$ kHz. Here the dephasing rates are $\gamma_{\text{dep}} \simeq 2\pi \times 1.3$ kHz, $2\pi \times 1.95$ kHz, and $2\pi \times 2.6$ kHz. Therefore, the scaling factor in Fig. 4 is $\gamma \simeq 2\pi \times 65$ kHz.

As shown in Fig. 4(a), we can definitely get spin squeezed for a relatively short evolution time. The system can always be in the spin squeezed state when $0 < t \leq \frac{0.8}{\gamma}$, and the squeezing parameter is about $\xi^2 \sim -10$ dB when $\Gamma_{a,b} \simeq 2\pi \times 0.065$ kHz and $\gamma_{\text{dep}} \simeq 2\pi \times 1.3$ kHz. Nevertheless, this nonclassical state will be destroyed because of the dissipation and dephasing. In Fig. 4(b), it is evident that the dissipation and dephasing will reduce the squeezing degree, and it finally evolves into a thermal state.

To examine the feasibility of our scheme in realistic experiment, we now discuss the relevant available experimental parameters. The magnetic coupling strength between the cavity and a single NV center is about $g_i \sim 2\pi \times 10$ Hz. The dissipation rate of microwave cavities is about $\kappa_a, \kappa_b > 2\pi \times 1$ kHz. In the practical situation, we consider a spin ensemble of $N \sim 10^{12}$ NV centers coupled to the cavity, and the collective coupling strength satisfies $\sqrt{N}g_i \sim 2\pi \times 10$ MHz [52]. The

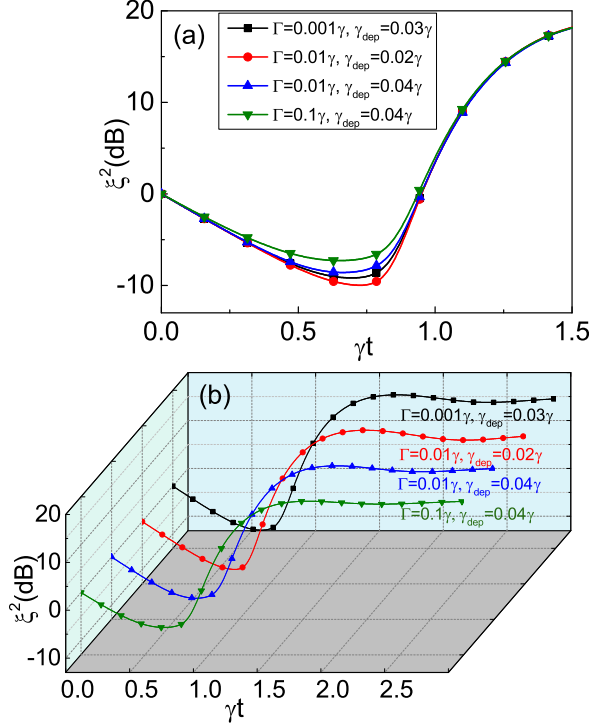


FIG. 4. (Color online) Time evolution of ξ^2 with H_T for $N \simeq 10^{12}$, where the parameters are chosen as $\lambda/\gamma \simeq 1$, $2\hbar/\gamma \simeq 0$ and the different effective dissipations are $\Gamma_a = \Gamma_b = \Gamma = 0.1\gamma, 0.01\gamma, 0.001\gamma$ and the dephasing rates are $\gamma_{dep} = 0.02\gamma, 0.03\gamma, 0.04\gamma$ respectively. (a) The evolution for a shorter time $0 \leq t \leq 1.5/\gamma$. (b) The evolution for a longer time $0 \leq t \leq 3/\gamma$.

Rabi frequency is about $|\Omega_i^*| \sim 2\pi \times 1$ MHz. Based on the chosen parameters, the time for maintaining the spin squeezed state is about $0 < t \leq 2 \mu\text{s}$ in this system, and we can obtain the degree of squeezing $\xi^2 \sim -10$ dB with the relative smaller number of the excitations. On the other hand, the relaxation time of the NV spin triplet ranging from milliseconds at room temperature to sev-

eral seconds at low temperature has been reported [53]. In addition, the dephasing time ($T_2 \propto 1/\gamma_{dep}$) more than $400 \mu\text{s}$ for spin ensemble has been demonstrated, and can be raised to about 2 ms with an isotopically pure diamond sample [62–66]. Thus, the coherence time is sufficient for achieving the desired spin squeezed state.

V. CONCLUSION

In summary, with the assistance of classical microwave fields and superconducting coplanar waveguide super-modes, we implement an exquisite setup for simulating LMG model with an NV center ensemble in diamond. Utilizing this hybrid quantum system, we can not only achieve the second order quantum phase transition when the coefficient satisfies $\lambda = \lambda_c$, but also prepare the spin squeezed state via the LMG Hamiltonian with the form of two-axis counter-twisting spin-spin interactions. In this protocol, due to the weak single coupling coefficient $g_i \ll \kappa_i$, the two-axis counter-twisting interactions will not be valid unless $N > 10^{10}$. Moreover, in spite of the negative effect of dissipations and dephasing, the squeezing degree is near to -10 dB when we choose $N \simeq 10^{12}$. We can further enhance the squeezing degree by increasing the number of the NV centers. Furthermore, if we extend this scheme to the LMG “Lattice” model, there will be more physics. This scheme is a new attempt for utilizing the hybrid quantum system to simulate the LMG model.

ACKNOWLEDGMENTS

This work is supported by the NSFC under Grant Nos. 11774285, 11474227 and 11534008, as well as the Fundamental Research Funds for the Central Universities. Part of the simulations are coded in PYTHON using the QUTIP library [67, 68].

[1] J. Verdú, H. Zoubi, Ch. Koller, J. Majer, H. Ritsch, and J. Schmiedmayer, Phys. Rev. Lett. **103**, 043603 (2009).
[2] Kathrin Henschel, Johannes Majer, Jörg Schmiedmayer, and Helmut Ritsch, Phys. Rev. A **82**, 033810 (2010).
[3] Anders Sørensen and Klaus Mølmer, Phys. Rev. Lett. **82**, 1971 (1999).
[4] J. I. Cirac and P. Zoller, Phys. Rev. Lett. **74**, 4091 (1995).
[5] Klaus Mølmer and Anders Sørensen, Phys. Rev. Lett. **82**, 1835 (1999).
[6] D. M. Meekhof, C. Monroe, B. E. King, W. M. Itano, and D. J. Wineland, Phys. Rev. Lett. **76**, 1796 (1996).
[7] Motoaki Bamba, Kunihiro Inomata, and Yasunobu Nakamura, Phys. Rev. Lett. **117**, 173601 (2016).
[8] M. Stern, G. Catelani, Y. Kubo, C. Grezes, A. Bienfait, D. Vion, D. Esteve, and P. Bertet, Phys. Rev. Lett. **113**,

123601 (2014).
[9] Andrew A. Houck, Hakan E. Türeci, and Jens Koch, Nat. Phys. **8**, 292 (2012).
[10] Peng-Bo Li, Ze-Liang Xiang, Peter Rabl, and Franco Nori, Phys. Rev. Lett. **117**, 015502 (2016).
[11] Alessio Serafini, Stefano Mancini, and Sougato Bose, Phys. Rev. Lett. **96**, 010503 (2006).
[12] Paolo Solinas, Pedro Ribeiro, and Rémy Mosseri, Phys. Rev. A **78**, 052329 (2008).
[13] R. G. Unanyan and M. Fleischhauer, Phys. Rev. Lett. **90**, 133601 (2003).
[14] Jian Ma and Xiaoguang Wang, Phys. Rev. A **80**, 012318 (2009).
[15] H. J. Lipkin, N. Meshkov, and A. J. Glick, Nucl. Phys. **62**, 188 (1965).

- [16] Julien Vidal, Rémy Mosseri, and Jorge Dukelsky, *Phys. Rev. A* **69**, 054101 (2004).
- [17] Julien Vidal, Guillaume Palacios, and Rémy Mosseri, *Phys. Rev. A* **69**, 022107 (2004).
- [18] José I. Latorre, Román Orús, Enrique Rico, and Julien Vidal, *Phys. Rev. A* **71**, 064101 (2005).
- [19] Masahiro Kitagawa and Masahito Ueda, *Phys. Rev. A* **47**, 5138 (1993).
- [20] T. Takano, M. Fuyama, R. Namiki, and Y. Takahashi, *Phys. Rev. Lett.* **102**, 033601 (2009).
- [21] Yong-Chang Zhang, Xiang-Fa Zhou, Xingxiang Zhou, Guang-Can Guo, and Zheng-Wei Zhou, *Phys. Rev. Lett.* **118**, 083604 (2017).
- [22] Y. C. Liu, Z. F. Xu, G. R. Jin, and L. You, *Phys. Rev. Lett.* **107**, 013601 (2011).
- [23] S. Morrison and A. S. Parkins, *Phys. Rev. Lett.* **100**, 040403 (2008).
- [24] Sheng-li Ma, Peng-bo Li, Ai-ping Fang, Shao-yan Gao, and Fu-li Li, *Phys. Rev. A* **88**, 013837 (2013).
- [25] Peng-Bo Li, Shao-Yan Gao, Hong-Rong Li, Sheng-Li Ma, and Fu-Li Li, *Phys. Rev. A* **85**, 042306 (2012).
- [26] Peng-Bo Li, Yong-Chun Liu, S.-Y. Gao, Ze-Liang Xiang, Peter Rabl, Yun-Feng Xiao, and Fu-Li Li, *Phys. Rev. Applied* **4**, 044003 (2015).
- [27] Peng-Bo Li, Shao-Yan Gao, and Fu-Li Li, *Phys. Rev. A* **83**, 054306 (2011).
- [28] Zhang-qi Yin, Tongcang Li, Xiang Zhang, and L. M. Duan, *Phys. Rev. A* **88**, 033614 (2013).
- [29] Ming Gao, Chun-Wang Wu, Zhi-Jiao Deng, Wen-Jie Zou, Li-gong Zhou, Cheng-Zu Li, and Xiang-Bin Wang, *Phys. Lett. A* **376**, 595 (2012).
- [30] Yu Zhou, Abdullah Rasmita, Ke Li, Qihua Xiong, Igor Aharonovich, and Wei-bo Gao, *Nat. Commun.* **8**, 14451 (2017).
- [31] Keyu Xia and Jason Twamley, *Phys. Rev. B* **94**, 205118 (2016).
- [32] Hua Wu, Richard E. George, Janus H. Wesenberg, Klaus Mølmer, David I. Schuster, Robert J. Schoelkopf, Kohei M. Itoh, Arzhang Ardavan, John J. L. Morton, and G. A. Briggs, *Phys. Rev. Lett.* **105**, 140503 (2010).
- [33] W. L. Yang, Zhang-qi Yin, Z. X. Chen, Su-Peng Kou, M. Feng, and C. H. Oh, *Phys. Rev. A* **86**, 012307 (2012).
- [34] J. H. Wesenberg, A. Ardavan, G. A. D. Briggs, J. J. L. Morton, R. J. Schoelkopf, D. I. Schuster, and K. Mølmer, *Phys. Rev. Lett.* **103**, 070502 (2009).
- [35] W. L. Yang, Z. Q. Yin, Y. Hu, M. Feng, and J. F. Du, *Phys. Rev. A* **84**, 010301(R) (2011).
- [36] Ze-Liang Xiang, Sahel Ashhab, J. Q. You, and Franco Nori, *Rev. Mod. Phys.* **85**, 623 (2013).
- [37] A. O. Niskanen, K. Harrabi, F. Yoshihara, Y. Nakamura, S. Lloyd, and J. S. Tsai, *Science* **316**, 723 (2007).
- [38] P. Rabl, D. DeMille, J. M. Doyle, M. D. Lukin, R. J. Schoelkopf, and P. Zoller, *Phys. Rev. Lett.* **97**, 033003 (2006).
- [39] Y. Kubo, C. Grezes, A. Dewes, T. Umeda, J. Isoya, H. Sumiya, N. Morishita, H. Abe, S. Onoda, T. Ohshima, V. Jacques, A. Dréau, J.-F. Roch, I. Diniz, A. Auffeves, D. Vion, D. Esteve, and P. Bertet, *Phys. Rev. Lett.* **107**, 220501 (2011).
- [40] Marcus W. Doherty, Neil B. Manson, Paul Delaney, Fedor Jelezko, Jörg Wrachtrup, and Lloyd C.L. Hollenberg, *Phys. Rep.* **528**, 1 (2013).
- [41] E. R. MacQuarrie, T. A. Gosavi, N. R. Jungwirth, S. A. Bhawe, and G. D. Fuchs, *Phys. Rev. Lett.* **111**, 227602 (2013).
- [42] Xiaobo Zhu, Shiro Saito, Alexander Kemp, Kosuke Kakuyanagi, Shin-ichi Karimoto, Hayato Nakano, William J. Munro, Yasuhiro Tokura, Mark S. Everitt, Kae Nemoto, Makoto Kasu, Norikazu Mizuochi, and Kouichi Semba, *Nature (London)* **478**, 221 (2011).
- [43] C. Zu, W.-B. Wang, L. He, W.-G. Zhang, C.-Y. Dai, F. Wang, and L.-M. Duan, *Nature (London)* **514**, 72 (2014).
- [44] P. Rabl, S. J. Kolkowitz, F. H. L. Koppens, J. G. E. Harris, P. Zoller, and M. D. Lukin, *Nat. Phys.* **6**, 602 (2010).
- [45] S. D. Bennett, N. Y. Yao, J. Otterbach, P. Zoller, P. Rabl, and M. D. Lukin, *Phys. Rev. Lett.* **110**, 156402 (2013).
- [46] Xin-You Lü, Ze-Liang Xiang, Wei Cui, J. Q. You, and Franco Nori, *Phys. Rev. A* **88**, 012329 (2013).
- [47] Ze-Liang Xiang, Xin-You Lü, Tie-Fu Li, J. Q. You, and Franco Nori, *Phys. Rev. B* **87**, 144516 (2013).
- [48] Kae Nemoto, Michael Trupke, Simon J. Devitt, Ashley M. Stephens, Burkhard Scharfenberger, Kathrin Buczak, Tobias Nöbauer, Mark S. Everitt, Jörg Schmiedmayer, and William J. Munro, *Phys. Rev. X* **4**, 031022 (2014).
- [49] W. L. Yang, Y. Hu, Z. Q. Yin, Z. J. Deng, and M. Feng, *Phys. Rev. A* **83**, 022302 (2011).
- [50] R. Amsüss, Ch. Koller, T. Nöbauer, S. Putz, S. Rotter, K. Sandner, S. Schneider, M. Schramböck, G. Steinhauser, H. Ritsch, J. Schmiedmayer, and J. Majer, *Phys. Rev. Lett.* **107**, 060502 (2011).
- [51] W. L. Yang, Z. Q. Yin, Q. Chen, C. Y. Chen, and M. Feng, *Phys. Rev. A* **85**, 022324 (2012).
- [52] Y. Kubo, F. R. Ong, P. Bertet, D. Vion, V. Jacques, D. Zheng, A. Dréau, J.-F. Roch, A. Auffeves, F. Jelezko, J. Wrachtrup, M. F. Barthe, P. Bergonzo, and D. Esteve, *Phys. Rev. Lett.* **105**, 140502 (2010).
- [53] P. Neumann, N. Mizuochi, F. Rempp, P. Hemmer, H. Watanabe, S. Yamasaki, V. Jacques, T. Gaebel, F. Jelezko, and J. Wrachtrup, *Science* **320**, 1326 (2008).
- [54] D. Marcos, M. Wubs, J. M. Taylor, R. Aguado, M. D. Lukin, and A. S. Sørensen, *Phys. Rev. Lett.* **105**, 210501 (2010).
- [55] P. Haikka, Y. Kubo, A. Bienfait, P. Bertet, and K. Mølmer, *Phys. Rev. A* **95**, 022306 (2017).
- [56] Yue Ma, Thai M. Hoang, Ming Gong, Tongcang Li, and Zhang-qi Yin, *Phys. Rev. A* **96**, 023827 (2017).
- [57] Jia-Bin You, W. L. Yang, Zhen-Yu Xu, A. H. Chan, and C. H. Oh, *Phys. Rev. B* **90**, 195112 (2014).
- [58] Wanlu Song, Wanli Yang, Junhong An, and Mang Feng, *Opt. Express* **25**, 19226 (2017).
- [59] L. J. Zou, D. Marcos, S. Diehl, S. Putz, J. Schmiedmayer, J. Majer, and P. Rabl, *Phys. Rev. Lett.* **113**, 023603 (2014).
- [60] D. F. V. James and J. Jerke, *Can. J. Phys.* **85**, 625 (2007).
- [61] Jian Ma, Xiaoguang Wang, C. P. Sun, and Franco Nori, *Phys. Rep.* **509**, 89 (2011).
- [62] Gopalakrishnan Balasubramanian, Philipp Neumann, Daniel Twitchen, Matthew Markham, Roman Kolesov, Norikazu Mizuochi, Junichi Isoya, Jocelyn Achard, Johannes Beck, Julia Tissler, Vincent Jacques, Philip R. Hemmer, Fedor Jelezko, and Jörg Wrachtrup, *Nat. Mater.* **8**, 383 (2009).
- [63] J. M. Taylor, P. Cappellaro, L. Childress, L. Jiang, D. Budker, P. R. Hemmer, A. Yacoby, R. Walsworth and M. D. Lukin, *Nat. Phys.* **4**, 810 (2009).

- [64] Jiangfeng Du, Xing Rong, Nan Zhao, Ya Wang, Jiahui Yang and R. B. Liu, *Nature (London)* **461**, 1265 (2009).
- [65] Susumu Takahashi, Ronald Hanson, Johan van Tol, Mark S. Sherwin, and David D. Awschalom, *Phys. Rev. Lett.* **101**, 047601 (2008).
- [66] P. L. Stanwix, L. M. Pham, J. R. Maze, D. Le Sage, T. K. Yeung, P. Cappellaro, P. R. Hemmer, A. Yacoby, M. D. Lukin, and R. L. Walsworth, *Phys. Rev. B* **82**, 201201(R) (2010).
- [67] J.R.Johansson, P.D.Nation, and Franco Nori, *Comput. Phys. Commun.* **183**, 1760 (2012).
- [68] J.R.Johansson, P.D.Nation, and Franco Nori, *Comput. Phys. Commun.* **184**, 1234 (2013).